BIOCHEMISTRY
including biophysical chemistry & molecular biology

Article

pubs.acs.org/biochemistry

Prion versus Doppel Protein Misfolding: New Insights from Replica-Exchange Molecular Dynamics Simulations

Pascal Baillod,[†] Julian Garrec,[†,‡] Ivano Tavernelli,[†] and Ursula Rothlisberger*[,†]

[†]Laboratory of Computational Chemistry and Biochemistry, Ecole Polytechnique Fédérale de Lausanne, 1015 Lausanne, Switzerland
[‡]CNRS, UMR 7565 Structure et Réactivité des Systèmes Moléculaires Complexes, Nancy Université, Nancy, France

Supporting Information

ABSTRACT: The doppel (Dpl) and prion (PrP) proteins share a very similar fold (three helices and two short β-strands), while they differ significantly in sequence (only 25% homologous) and in disease-related β-rich conformations that occur for PrP only. In a previous study [Baillod, P., et al. (2012) *Biochemistry 51*, 9891−9899], we investigated the misfolding and rare, β-rich folds of monomeric PrP with replica-exchange molecular dynamics (REMD) simulations. In the work presented here, we perform analogous simulations for Dpl with the aim of comparing the two systems and characterizing possible specificities of PrP for misfolding and amyloidogenesis. Our extensive simulations, which allow us to overcome high energy barriers via the REMD approach, sample several β-rich folds, some of which are stable at room temperature, for both proteins. Per residue secondary structure propensities reveal that novel β-sheets of Dpl and PrP are formed by amino acids belonging to the helices that are the least stable in the respective native structure, H1 for Dpl and H2 and H3 for PrP, in agreement with experimental data. Using a specific clustering method that allows discrimination against different β-strand arrangements, seven β-rich folds could be characterized for PrP and five for Dpl, which are clearly distinct and share only one single similar fold. A major difference between the two proteins is found in the free energy barriers leading to misfolded structures: they are approximately 3 times higher for Dpl than for PrP. This suggests that the difference in amyloidogenic behavior between PrP and Dpl might be due to kinetic reasons.

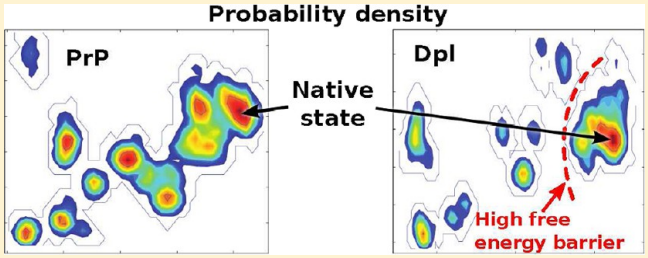

Creutzfeldt-Jakob disease (CJD), bovine spongiform encephalopathies (BSE), scrapie, and other transmissible spongiform encephalopathies (TSE) are related to the misfolding of the endogenous prion protein (PrP),[1−3] as revealed by the isolation[4] and sequencing[5−7] of PrP^{Sc}, an aggregated, infectious PrP isoform found in the central nervous system of infected organisms.

One of the first attempts to understand the function of PrP, which remains enigmatic,[8,9] was to create knockout mouse lines deficient in PrP ($PrP^{0/0}$). The first two $PrP^{0/0}$ lines, Zürich I[10] and Edinburgh,[11] were viable and phenotypically normal, suggesting that PrP function was not indispensable or can be taken over by another protein. However, animals of a third (*Ngsk* $PrP^{0/0}$)[12] and fourth (*Rcm0* $PrP^{0/0}$)[13] $PrP^{0/0}$ line developed late onset ataxia accompanied by Purkinje cell degeneration. Another strategy applied to the elucidation of PrP function consisted of searching for related genes. Large cosmid clones containing the PrP gene of different species were investigated, and a candidate was eventually found 16 kb downstream of the *Prnp* mouse PrP gene. The new gene, encoding a 179-residue protein with a sequence that is ∼25% identical with the sequences of all known prion proteins, was called Doppel (*PrnD* gene and Dpl protein), a German synonym for "double".[13]

PrP knockout cells have been shown to undergo Dpl-induced apoptosis in a dose-dependent manner.[14] Alternatively, Dpl toxicity might be related to oxidative stress, because Dpl was shown to induce expression of nitric oxide synthase (NOS)[15,16] and Dpl toxicity could be blocked by a NOS inhibitor.[15] Dpl-induced ataxia leads to a pathology that differs from PrP^{Sc}-induced TSE and is devoid of amyloid fibrils. Surprisingly, reintroduction of *Prnp* transgenes into $PrP^{0/0}$ lines suppressed the toxic effects caused by Dpl,[17] suggesting an antagonistic function of PrP in blocking the neurotoxicity of Dpl. The physical binding of the two proteins was demonstrated with an enzyme-linked immunosorbent assay in which PrP^{C}, bound to the plate, could bind Dpl.[15] PrP and Dpl were also shown to copatch at the plasma membrane and co-internalize in neuroblastoma cells.[18]

A nuclear magnetic resonance (NMR) structure was obtained for the full-length mouse Dpl, intriguingly revealing a fold that is very similar to that of the C-terminal domain of mouse PrP, with three helices (H1−H3) and two short β-strands (S1 and S2)[19] (Figure 1, panels labeled dNMR and p & dNMR). Small differences can be found in the β-strands

Received: July 5, 2013
Revised: October 18, 2013
Published: October 22, 2013

dx.doi.org/10.1021/bi400884e | *Biochemistry* 2013, 52, 8518−8526

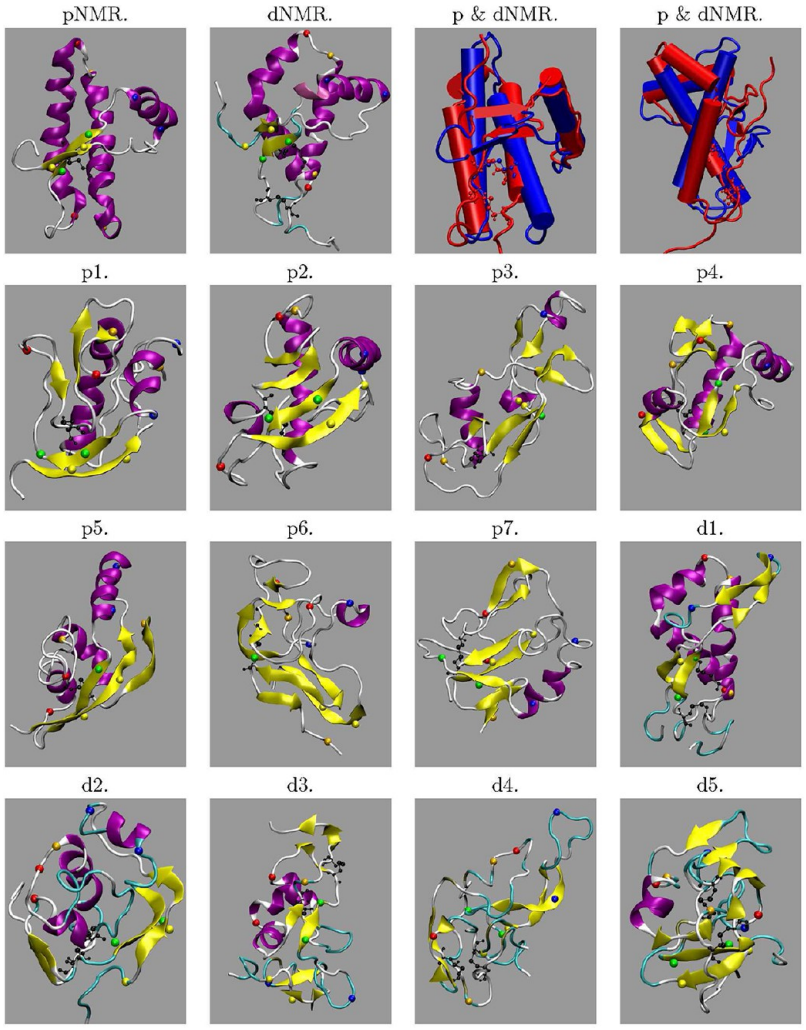

Figure 1. Representative structures of the main β-contact map clustering folds of PrP (p1−p7) and Dpl (d1−d5). Panels labeled pNMR and dNMR show the NMR structures of PrP and Dpl, respectively. The two panels labeled "p & dNMR" both show the structural superposition (90° rotated views) of these NMR structures (blue for PrP, red for Dpl). In all panels except those labeled "p & dNMR", (i) helices are colored purple and β-sheets yellow, (ii) to highlight the sequence positions of structural rearrangements, sequence portions spanning NMR secondary structure elements are highlighted with sphere representations of the C-α atoms of the residues delimiting S1 (yellow), S2 (green), H1 (blue), H2 (red), and H3 (orange), and (iii) the disulfide bridge-forming Cys residues are shown as black spheres for all the atoms.

(slightly shorter in Dpl), as well as in a kink of the second Dpl helix that contributes to a triangular hydrophobic pocket. Further similarities to PrP include the two glycosylation sites (Asn99 and Asn111, with sequence positions that differ from those of PrP and link different oligosaccharides) and a GPI anchor at Gly155.[20] In comparison with PrP, Dpl contains an extra disulfide bond. The first disulfide bond (Cys109 and Cys143) is analogous to that of PrP (Cys178 and Cys213) and connects H2 to H3. The second one connects the S2−H2 loop to a Cys of the flexible C-terminus of the protein (Cys95 and Cys148). The NMR structure of human Dpl is very similar to that of mouse Dpl, and the high degree of amino acid conservation suggests structural similarity between all mammalian Dpl proteins.[21]

Many PrP *in vitro* unfolding studies have been performed with the aim of understanding the misfolding process leading to the pathogenic PrP^{Sc} isoform, highlighting a number of misfolding pathways and β-rich conformations.[22−32] The relative free energy, ΔG^u, at 300 K between the native and thermally unfolded states can be estimated by applying the modified Gibbs−Helmholtz equation[33] to transition temperature midpoints (T_m) and van't Hoff enthalpies (ΔH^m) obtained from thermal unfolding experiments. Surprisingly, PrP with a single disulfide bridge was found to be thermally more stable ($T_m \sim 70$ °C, $\Delta H^m \sim 292$ kJ/mol, and $\Delta G^u \sim 26$ kJ/mol[34,35]) than Dpl with two disulfide bridges ($T_m \sim 53-58$ °C, $\Delta H^m \sim 192-205$ kJ/mol, and $\Delta G^u \sim 12$ kJ/mol[36,37]). This trend was confirmed by chemical unfolding experiments, resulting in ΔG^u values of 19.3 and 12.6 kJ/mol for PrP and Dpl, respectively.[36,38] Nicholson et al. observed superprotection in the H2−H3 segment in PrP (suggesting a partially structured unfolded state) but not in Dpl.[38] Moreover, neither wild-type Dpl nor a single-disulfide bridge mutant Dpl could be induced to exhibit the α to β transition that is typical of PrP to PrP^{Sc} conversion.[36] A slight increase in β-content was however obtained by co-incubating Dpl with negligible amounts of PrP106−126 (too small to produce any CD spectra).[15]

In a previous study, we applied extensive replica-exchange molecular dynamics (REMD) to investigate PrP misfolding.[39] These simulations allowed us to identify a pool of rare β-rich structures that were clustered into different folds according to the location and topology of the newly formed β-sheets. The

dx.doi.org/10.1021/bi400884e | *Biochemistry* 2013, 52, 8518−8526

aim of the study presented here is to apply an analogous simulation protocol to Dpl. Previous simulations of this protein (see, e.g., refs 40 and 41) focused on the characterization of its native state and its folding and unfolding using, e.g., high-temperature simulations. To the best of our knowledge, the study presented here is the first that reports a thorough exploration of conformational landscape of Dpl (including misfolded structures) at room temperature. To anticipate our results, we determine relative thermal stabilities for the two proteins that are in agreement with the results of unfolding experiments. Surprisingly, β-rich configurations are found for both proteins and not for PrP only. However, at 300 K, the free energy barriers separating the native structures from such states, as well as from other non-native states, are at least 3 times higher for Dpl. The characterization of Dpl misfolding and the identification of its β-rich folds highlight the difference in the conformational properties of this structural homologue of PrP. Furthermore, assessing sequence differences between Dpl and PrP that lead to differences in β-sheet and α-helical propensities or to different local folds, despite a very similar global native fold, can shed new light on the twilight zone separating mere unfolding from disease-related aggregation and amyloidogenesis.

METHODS

The protocol we used for this study is the same as that we used previously for our investigation of the misfolding of the prion protein.[39] Here, we briefly review the main aspects of our methodology and highlight the specificities of the simulations we performed for Dpl. We refer the reader to ref 39 for more details.

Molecular Dynamics Setup. The initial configuration we used for the simulations of Dpl was obtained from the NMR structure of mouse Dpl [Protein Data Bank (PDB) entry 1I17].[19] Like in ref 39, we modeled the system at pH 4, because acidic conditions are known to accelerate the conversion of PrP^{C} to $PrP^{Sc31,42-50}$ (see also ref 51 and the references cited therein).

We performed Poisson−Boltzmann calculations[52,53] to assign the protonation state of titratable residues, using the DELPHI program[54] supplied with the WHATIF[54] package.[55] According to these calculations, the protonation states were as follows: Glu4, d; Asp18, p; Asp20, d; Glu24, d; Asp38, d; Glu43, d; Glu47, p; Glu53, p; Glu70, d; Glu74, d; Asp77, p; His81, p; Glu91, d; His97, p; Asp99, p; and Glu103, p (where p stands for protonated and d for deprotonated).

All simulations were performed with the GROMACS 3.3.0 package,[56] the GROMOS96 43a1 force field,[57] and the SPC explicit solvent water model.[58] All MD simulation parameters were kept the same as in ref 39.

Reference Molecular Dynamics Simulation. A 315 ns reference MD simulation was run in the *NVT* ensemble. Such a simulation was performed in our previous study of PrP[39] (i) to check the validity of our REMD protocol (see the next section) and (ii) to assess its performance in terms of configurational sampling with respect to straightforward MD simulations. Here, we mainly use this reference simulations to establish a first comparison between PrP and Dpl.

REMD Simulations. To enhance the conformational sampling, we used the same hybrid REMD protocol[59,60] as in ref 39. Briefly, the equations of motion at each temperature are propagated using a standard MM potential with explicit solvent, while Monte Carlo switching probabilities between the different replica are computed using the protein potential energy only (including its energy of interaction with the solvent) instead of the full potential. Previous studies have shown that the effect of this type of approximation on the final sampling is negligible.[59,61,62] The REMD simulations were conducted using 32 replicas with the following temperature distribution: 300.0, 306.0, 312.1, 318.2, 324.3, 330.4, 336.6, 342.8, 349.1, 355.3, 361.6, 368.0, 374.3, 380.7, 387.1, 393.6, 400.1, 406.6, 413.1, 419.7, 426.3, 432.9, 439.6, 446.3, 453.0, 459.8, 466.5, 473.3, 480.2, 487.1, 494.0, and 500.9 K.

The simulation length was 56.4 ns for each replica (corresponding to a total time of 1.8 μs). It was chosen on the basis of our previous convergence analysis performed in ref 39 using the fact that, after tens of nanoseconds, we do not seem to sample a significant amount of new conformational clusters. This is illustrated by the time evolution of the fraction of collapsed structures that reaches a plateau at the end of the simulation (Figure S4 of ref 39). We stress that the main goal of our study is a thorough and extended exploration of the conformational landscape of PrP and Dpl, more than reaching ergodicity (which is most probably impossible in this case). As discussed in Results and Discussion, our simulations are long enough to highlight possible misfolded structures at room temperature for both proteins and to show that the topologies of their conformational landscapes differ substantially (Figure 5) despite the high degree of structural similarity of their native states. In addition, the agreement of our results with a broad range of experimental data [in particular the relative stability of the helices and the relative thermal stability of PrP and Dpl (see Results and Discussion)] strongly suggests that our simulations provide a realistic description of PrP and Dpl.

Conformational Landscape and Free Energy Barriers. Following the spirit of ref 39, the conformations obtained from our REMD simulations were used to compute the probability distribution as a function of a set of order parameters, which served as a fingerprint of the conformational landscape of a given protein. We tested several pairs of order parameters and found that the radius of gyration (R_g) and the fraction of native contacts (Q_N) taken together were the best to highlight and distinguish key conformational basins for Dpl and PrP [the corresponding probability distributions, $P(Q_N,R_g)$, are represented in panels 1 and 2 of Figure 5, respectively]. In particular, the choice of R_g is relevant for PrP because, as highlighted in ref 39, a significant portion of the conformational landscape explored by our REMD simulations is characterized by collapsed structures with respect to the native state. This is in agreement with high-pressure unfolding experiments in which PrP was observed to collapse around molecular voids.[30]

To compare the misfolding propensity of PrP and Dpl, we estimated the free energy barriers surrounding the native state in the two systems. To do so, we converted the probability distributions in free energy landscapes, $\Delta G(Q_N,R_g)$, using the following expression:[63]

$$\Delta G_{A\to B} = G(Q_N^B, R_g^B) - G(Q_N^A, R_g^A) = -RT \ln \frac{P(Q_N^B, R_g^B)}{P(Q_N^A, R_g^A)} \quad (1)$$

where A and B are two states characterized by specific values of Q_N and R_g. It should be stressed that using this strategy to compute free energy barriers can yield only approximate results here. First, our REMD simulations provide only a limited

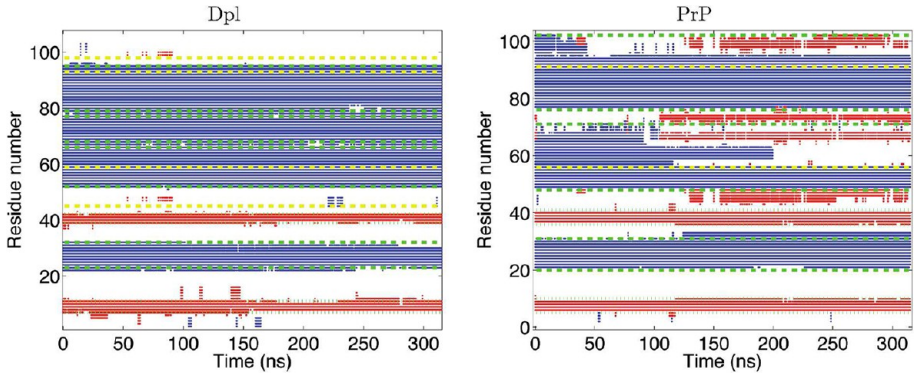

Figure 2. Secondary structure (DSSP) as a function of time in our reference MD simulations of Dpl (left) and PrP (right). Color coding for the secondary structure: red for β-sheet and blue for α-helix. Native (NMR) secondary structure element locations are delimited by dashed and dotted green horizontal lines: dotted for β-sheets (in sequence order, S1 and S2) and dashed for α-helices (in sequence order, H1, H2a, H2b, and H3 for Dpl and H1, H2, and H3 for PrP). Yellow dashed horizontal lines denote Cys residues forming disulfide bridges. Residues were numbered starting from the first residue of the NMR PDB file.

sampling of transition regions associated with high free energy barriers (white regions in panels 1 and 2 of Figure 5). As a consequence, the free energy landscape obtained from eq 1 is statistically inaccurate in transition regions and cannot be used directly to compute free energy barriers. Fortunately, the REMD approach allows an extensive sampling of the free energy basins (colored ones in panels 1 and 2 of Figure 5) that are connected by these transition regions. Thus, it is still possible to fit parabolae along the lowest-free energy path in these basins and to extrapolate the free energy profile to regions of low probability. Then, the intersection point of these parabolae can serve as an approximation for the transition state and provides an upper bound for the free energy barrier. Although this is a rough estimate, repeating this operation for both PrP an Dpl allows an insightful comparison to be made.

Second, it is worth stressing that when choosing the radius of gyration (R_g) and the fraction of native contacts (Q_N) as a set of order parameters for computing free energy barriers, we implicitly define a state i as an ensemble of conformations for which R_g and Q_N take specific values, $\{Q_N^i, R_g^i\}$. Choosing another set of order parameters would change the shape of the probability distributions as well as the corresponding free energy landscape. This means that the absolute values of free energy barriers computed using the method mentioned above should be considered with caution. Nevertheless, it turns out that the estimated barriers are always higher for Dpl than for PrP [with a ratio of ~3 (see also Results and Discussion)], which is independent of the choice of order parameters. Hence, we use this method more as a way to provide a qualitative, yet insightful, comparative analysis about the kinetics of PrP and Dpl misfolding, rather than to compute absolute free energy barriers.

Secondary Structure Analysis and Clustering. Structural analysis and clustering analysis were performed as described in ref 39. Briefly, the secondary structure of each configuration generated by our REMD simulations was defined with the DSSP[64] algorithm. Then, for each β-rich configuration (i.e., those containing $\geq$19 β-residues), a β-contact map (bcm) was computed. This map represents the contacts between different β-strands in a given configuration and so is the fingerprint of the β-strand arrangement in that configuration. Finally, the bcm's of all β-rich configurations are clustered to yield a series of β-rich folds.

RESULTS AND DISCUSSION

Reference MD Simulations. As a first comparison between PrP and Dpl, we performed 315 ns standard (i.e., without enhanced sampling) reference MD simulations for both proteins. Dpl shows a very high stability, characterized by the conservation of all native secondary structure elements throughout the simulation (Figure 2, left panel). In stark contrast, in the PrP simulation, H2 and H3 partially unfold between 45 and 200 ns and two additional β-sheets are formed (Figure 2, right panel). The corresponding partially misfolded structure is represented in panel p4 of Figure 1 [it is also observed in our REMD simulations (see the following sections)].

As mentioned in our previous investigation of PrP,[39] we intentionally chose simulation conditions such as acidic pH (pH 4) and the GROMOS force field[39] that can be expected to accelerate conformational transitions to β-rich structures. Indeed, the GROMOS force field is known to favor β-sheets with respect to α-helices.[65] However, because we applied exactly the same protocol to PrP and Dpl, the relative differences that we observe for the two systems can be expected to be independent of possible limitations related to the force field. The comparison of the simulation results for the two systems suggests that PrP has an intrinsically higher propensity for the formation of alternative folds than Dpl.

However, because of the limited sampling time, straightforward MD cannot be considered to be fully conclusive with respect to the presence or absence of free energy barriers. That is why our study mainly applies REMD (see the next section). The main advantage of this approach is that it allows us to overcome high energy barriers that the system has to cross to convert from one fold (e.g., the native state) to another (e.g., a misfolded state), because of the large temperature interval that the simulation replicas span.[39]

Thermal Stability from REMD Simulations. For a more comprehensive picture of the overall conformational landscape of PrP and Dpl, we performed extensive explicit solvent REMD simulations. In the remainder of this paper, we will focus on the results obtained from these enhanced sampling simulations. As a first result of our REMD simulations, we compared the thermal stability of the two proteins, assessed by the fraction of native versus non-native structures present at different REMD temperatures. For both proteins, native structures were defined

dx.doi.org/10.1021/bi400884e | Biochemistry 2013, 52, 8518−8526

as structures with ≥64% native contacts present in the respective NMR structures. We have chosen this cutoff because we found that PrP structures satisfying this criterion share many structural traits with the native state, in particular the conservation of the three helices (although their length may vary) and the two β-strands.

The average fractions of native structures per temperature show a higher thermal stability for PrP than for Dpl (Figure 3),

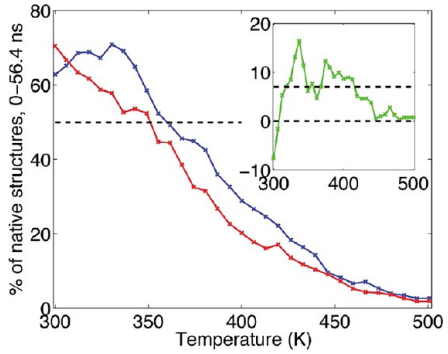

Figure 3. Average fractions of native structures as a function of temperature for PrP (blue) and Dpl (red). The dashed line shows 50% of native structures. The inset shows differences between the fractions of native structures for PrP and Dpl. The gray dashed line shows 0% and the black dashed like 7% (average difference in the temperature range of 300−439 K). Structures with a threshold of ≥64% of the native contacts are defined as being native.

in agreement with experiments.[34−38] An exception is found at a low temperature (~300 K), for which the fractions of native structures are slightly lower for PrP than for Dpl. This is due to the fact that PrP can loose nativelike structures at very low temperatures in favor of β-enriched conformations, consistent with our reference MD simulations.

Secondary Structure Propensities. Besides the mere loss of native structure at elevated temperatures, new β-sheets form on rare occasions for both proteins during the REMD simulations. Of all the sampled conformations (at all temperatures), 1.3% of PrP and 2.7% of Dpl structures have a β-content of ≥19 residues. Although β-structure enrichment was not observed in Dpl thermal unfolding studies,[36] β-rich conformations might be favored by other denaturing conditions. Indeed, a number of proteins that are not involved in amyloidogenesis-related diseases show β-rich states under a variety of denaturing conditions.[66−70]

To compare the secondary structure propensity of PrP and Dpl sequences, we defined the per-residue secondary structure propensity by the fraction of simulation time that each residue spends in α-helical or β-sheet conformations, at a given temperature (Figure 4). As we have shown in ref 39 (see also the bottom left panel of Figure 4), for PrP, H2 is found to be the least stable helix at all temperatures, followed by H3 and H1, consistent with the results from the 300 K reference MD simulation, experimental stability studies,[30,45,71−74] and predictions from previous simulations.[48,51,75−78] For Dpl (Figure 4, top left panel), the pattern differs strongly. H1 is the least stable helix, followed by H2 and H3.

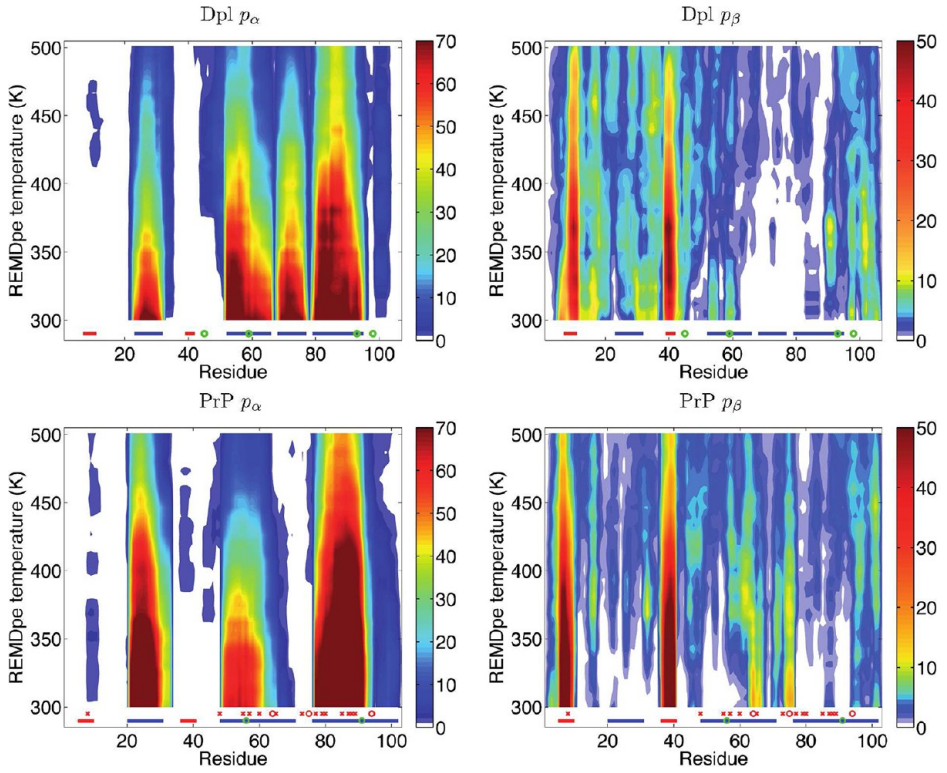

Figure 4. Per residue α-helical propensity (p_α) and per residue β sheet propensity (p_β), computed as the percentage (color bar) of time spent by each residue at different REMD temperatures in the α- or β-conformation. The first (i) and second (ii) colored rulers just above the x-axis show (i) NMR α-helices (blue) and β-sheets (red) (solid lines), with green circles indicating the location of the disulfide bridge-forming Cys residues, and (ii) mutations favoring prion diseases:[79] red x (mutations increasing hydrophobicity) and red o (mutations decreasing hydrophobicity) (shown for PrP only). Residues were numbered starting from the first residue of the NMR PDB file.

dx.doi.org/10.1021/bi400884e | *Biochemistry* 2013, 52, 8518−8526

In addition, the location of the newly formed β-sheets differs for the two proteins (Figure 4, right column). In PrP, β-sheets are mainly formed by residues belonging to H2 and H3 in the native structure. This sequence interval contains most of the disease-promoting mutations,[79] as well as the "β-core" of residues for which three different independent experiments suggest the involvement in a PrP^{Sc} β-sheet scaffold.[72,80,81] New β-sheets in Dpl are mainly formed in the sequence interval delimited by the protein N-terminus and the native β-strand S2, where residues of the unstable H1 helix become available, in contrast to PrP, where these residues remain in a helical conformation most of the time.

β-Rich Folds. In ref 39, we introduced the β-contact map clustering (bcmc) protocol (see Methods), developed to identify the main β-rich folds in the β-rich pool of structures with at least 19 residues in the β-conformation in the PrP REMD simulation. In the work presented here, we apply an identical bcmc protocol to the β-rich pool observed during the Dpl REMD simulation and compare the main β-rich folds of PrP and Dpl. Representative structures are shown in Figure 1. Seven and five main β-rich folds were found for PrP and Dpl, respectively, at room temperature. PrP folds have been discussed previously in relation to recent PrP misfolding experiments.[39] A comparison of the PrP β-rich folds with those of Dpl shows that there are very few common trends: only Dpl fold 2 (d2) and PrP fold 4 (p4) resemble each other to some degree.

In ref 39, we suggested that p4 might be related to a precursor of the β-oligomeric form, a stable and soluble PrP conformation that has been reported to form on the time scale of hours to days in stock solutions without prior denaturing treatment.[23] It has even been suggested that this structure corresponds to the free energy minimum in aqueous solution.[26,27,82] In ref 39, we also analyzed whether the PrP β-rich folds contained a sufficient amount of α-helical residues to be consistent with experimental determinations of the α-helical content of PrP^{Sc}. β-Rich folds containing at least one structure with $\geq$17 α-helical residues were termed α+, while those β-rich folds with <17% α-helical content were termed $\alpha-$. Although in the case of Dpl, such a distinction is not motivated by direct experimental results, we apply the same classification scheme to Dpl for the sake of comparison. It turns out that in the case of Dpl, most of the β-rich structures belong to an α-fold, in contrast to PrP (Table 1). This finding is consistent with the thermal stability (related to the helical content), which was found to be lower for Dpl than for PrP.[34−37] It also supports the idea that PrP can progressively unfold into β-rich states while maintaining a large part of its α-helical topology facilitating misfolding with respect to other proteins, while Dpl would need to overcome a higher energy barrier (see the next section) corresponding to the disruption of most of its helical content to access a β-rich state.

Table 1. Fractions (%) of β-Rich Pools Found in the Main bcmc Folds (F) of Dpl and PrP[a]

	Dpl		Prp	
	F	%	F	%
α+	1	5.7	1	17
	2	5.5	2	0.9
	3	0.7	3	8.9
			4	16.6
			5	0.8
$\alpha-$	4	39.9	6	9.9
	5	14.9	7	2.2

[a] α+ refers to the folds that contain at least one structure with $\geq$17 α-helical residues and $\alpha-$ to folds that comprise no such structure.

Kinetic Trapping. The extended conformational space explored for both proteins is represented by the probability distributions projected on the fraction of native contacts and the radius of gyration (Figure 5). The high-temperature probability distributions of PrP and Dpl are very similar (Figure 5, panel 4) and converge to a new, non-native, and more compact structure. In contrast, the 300 K probability distributions differ for the two proteins (Figure 5, panel 3): while PrP reveals a succession of connected high-probability regions leading from the native state to a non-native compact form (Figure 5, panel 2), the corresponding high-probability regions in Dpl are well separated from one another (Figure 5, panel 1). This indicates high free energy barriers for Dpl, which are crossed only with the help of the enhanced sampling provided by REMD. In particular, the native Dpl population is isolated by such barriers on the free energy surface, suggesting that the protein must be particularly stable toward misfolding in the absence of denaturing conditions (high temperature, detergents, etc.). We estimate that the barriers in the case of Dpl are approximately 3 times higher than the corresponding barriers in PrP (see Methods for more details). Thus, in agreement with our reference MD 300 K simulations, the REMD 300 K simulations also show a higher kinetic stability for Dpl than for PrP.

CONCLUSIONS

In this work, REMD simulations of misfolding and of rare β-rich conformations of PrP and of its nonpathogenic structural homologue Dpl are compared, with the aim of highlighting PrP specific misfolding characteristics that might relate to PrP pathologies. In agreement with experiments, we find a higher thermal stability for PrP than for Dpl. However, for Dpl, the free energy barriers leading to non-native and β-rich states are at least 3 times higher than for PrP, suggesting a higher kinetic stability for the former. Indeed, although both proteins can access β-rich conformations via thermal misfolding (high REMD temperatures), only PrP can readily convert into the β-rich misfold p4 via long (~100 ns) straightforward reference MD simulations at 300 K, whereas β-rich folds can be observed only in enhanced sampling simulations of Dpl. This difference suggests a higher intrinsic misfolding and β-enrichment propensity for PrP than for Dpl.

The β-cores observed in the β-rich folds for both PrP and Dpl are formed by residues belonging to the helices that are the least stable in the corresponding native structures: H2 and H3 for PrP and H1 for Dpl. Thus, the stability of the helices, related to the sequence, appears as a determinant of the β-propensity and β-folds that can be formed. Seven β-rich folds are found for PrP and five for Dpl, with one single quasi-common fold, p4/d2, that accumulates at 300 K in the PrP REMD simulation and is also formed in the PrP reference MD simulation at the same temperature. This stable β-rich misfold is therefore accessible from two different amino acid sequences, suggesting a sequence-independent stabilization process and a possible relation to soluble PrP β-oligomers formed under certain experimental conditions and found to be even more stable than the native structure.[26,27,82] Finally, the fact that there are practically no common β-rich folds in PrP and Dpl

dx.doi.org/10.1021/bi400884e | Biochemistry 2013, 52, 8518−8526

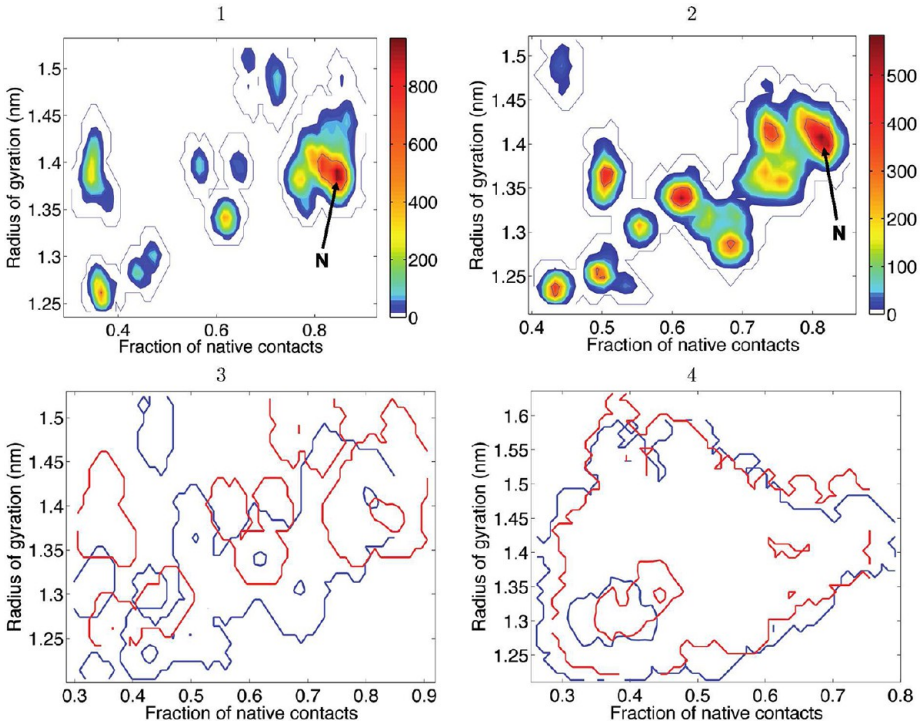

Figure 5. Probability distributions computed as a function of the fraction of native contacts and the radius of gyration: (1) Dpl at 300 K and (2) PrP at 300 K. Color bars in panels 1 and 2 report the number of structures. Two solid contour lines are added to panels 1 and 2: an outer one to encompass the maximal extent of non-zero probability regions (≥1 count) and an inner one at half of the maximal count observed to highlight high-probability regions. The native state of each protein is indicated by the letter N. Analogue contour lines are drawn in panels 3 (300 K) and 4 (500 K) to compare the superposed probability distributions of Dpl (red) and PrP (blue).

suggests that if Dpl β-rich folds are at all possible under physiological conditions, they might not be related to amyloidogenic pathologies. In contrast, one or more of the PrP specific β-rich folds may represent monomeric PrP^{Sc} or PrP* precursor forms.[30]

■ ASSOCIATED CONTENT

Ⓢ Supporting Information

Representative structures of the conformational landscape of PrP. This material is available free of charge via the Internet at http://pubs.acs.org.

■ AUTHOR INFORMATION

Corresponding Author

*E-mail: ursula.roethlisberger@epfl.ch. Phone: +41-(0)21-693-0321. Fax: +41-(0)21-693-0320.

Funding

Swiss National Science Foundation Grant 200020-130082 is acknowledged for funding.

Notes

The authors declare no competing financial interest.

■ ACKNOWLEDGMENTS

We thank the DIT/EPFL, the CSCS, and the CADMOS project for the computer time.

■ ABBREVIATIONS

PrP, prion protein; PrP^{C}, cellular form of PrP; PrP^{Sc}, scrapie form of PrP; Dpl, doppel protein; REMD, replica-exchange molecular dynamics.

■ REFERENCES

(1) Prusiner, S. B. (1998) Prions. *Proc. Natl. Acad. Sci. U.S.A. 95*, 13363−13383.

(2) Aguzzi, A., and Calella, A. M. (2009) Prions: Protein aggregation and infectious diseases. *Physiol. Rev. 89*, 1105−1152.

(3) Soto, C. (2012) Transmissible proteins: Expanding the prion heresy. *Cell 149*, 968−977.

(4) Prusiner, S. (1982) Novel proteinaceous infectious particle causes scrapie. *Science 216*, 136−144.

(5) Oesch, B., Westaway, D., Wälchli, M., McKinley, M. P., Kent, S. B., Aebersold, R., Barry, R. A., Tempst, P., Teplow, D. B., and Hood, L. E. (1985) A cellular gene encodes scrapie PrP 27−30 protein. *Cell 40*, 735−746.

(6) Chesebro, B., Race, R., Wehrly, K., Nishio, J., Bloom, M., Lechner, D., Bergstrom, S., Robbins, K., Mayer, L., and Keith, J. M. (1985) Identification of scrapie prion protein-specific mRNA in scrapie-infected and uninfected brain. *Nature 315*, 331−333.

(7) Basler, K., Oesch, B., Scott, M., Westaway, D., Wälchli, M., Groth, D. F., McKinley, M. P., Prusiner, S. B., and Weissmann, C. (1986) Scrapie and cellular PrP isoforms are encoded by the same chromosomal gene. *Cell 46*, 417−428.

(8) Westergard, L., Christensen, H. M., and Harris, D. A. (2007) The cellular prion protein (PrP^{C}): Its physiological function and role in disease. *Biochim. Biophys. Acta 1772*, 629−644.

(9) Caughey, B., and Baron, G. S. (2006) Prions and their partners in crime. *Nature 443*, 803−810.

(10) Büeler, H., Fischer, M., Lang, Y., Bluethmann, H., Lipp, H. P., DeArmond, S. J., Prusiner, S. B., Aguet, M., and Weissmann, C. (1992) Normal development and behaviour of mice lacking the neuronal cell-surface PrP protein. *Nature 356*, 577−582.

(11) Manson, J. C., Clarke, A. R., McBride, P. A., McConnell, I., and Hope, J. (1994) PrP gene dosage determines the timing but not the final intensity or distribution of lesions in scrapie pathology. *Neurodegeneration 3*, 331−340.

(12) Sakaguchi, S., Katamine, S., Nishida, N., Moriuchi, R., Shigematsu, K., Sugimoto, T., Nakatani, A., Kataoka, Y., Houtani, T., Shirabe, S., Okada, H., Hasegawa, S., Miyamoto, T., and Noda, T. (1996) Loss of cerebellar Purkinje cells in aged mice homozygous for a disrupted PrP gene. *Nature 380*, 528−531.
(13) Moore, R. C., et al. (1999) Ataxia in prion protein PrP-deficient mice is associated with upregulation of the novel PrP-like protein doppel. *J. Mol. Biol. 292*, 797−817.
(14) Sakudo, A., Lee, D. C., Nakamura, I., Taniuchi, Y., Saeki, K., Matsumoto, Y., Itohara, S., Ikuta, K., and Onodera, T. (2005) Cell-autonomous PrP-Doppel interaction regulates apoptosis in PrP gene-deficient neuronal cells. *Biochem. Biophys. Res. Commun. 333*, 448−454.
(15) Cui, T., Holme, A., Sassoon, J., and Brown, D. R. (2003) Analysis of doppel protein toxicity. *Mol. Cell. Neurosci. 23*, 144−155.
(16) Wong, B. S., Brown, D. R., Pan, T., Whiteman, M., Liu, T., Bu, X., Li, R., Gambetti, P., Olesik, J., Rubenstein, R., and Sy, M. S. (2001) Oxidative impairment in scrapie-infected mice is associated with brain metals perturbations and altered antioxidant activities. *J. Neurochem. 79*, 689−698.
(17) Nishida, N., Tremblay, P., Sugimoto, T., Shigematsu, K., Shirabe, S., Petromilli, C., Erpel, S. P., Nakaoke, R., Atarashi, R., Houtani, T., Torchia, M., Sakaguchi, S., DeArmond, S. J., Prusiner, S. B., and Katamine, S. (1999) A mouse prion protein transgene rescues mice deficient for the prion protein gene from Purkinje cell degeneration and demyelination. *Lab. Invest. 79*, 689−697.
(18) Massimino, M. L., Ballarin, C., Bertoli, A., Casonato, S., Genovesi, S., Negro, A., and Sorgato, M. C. (2004) Human Doppel and prion protein share common membrane microdomains and internalization pathways. *Int. J. Biochem. Cell Biol. 36*, 2016−2031.
(19) Mo, H., Moore, R. C., Cohen, F. E., Westaway, D., Prusiner, S. B., Wright, P. E., and Dyson, H. J. (2001) Two different neurodegenerative diseases caused by proteins with similar structures. *Proc. Natl. Acad. Sci. U.S.A. 98*, 2352−2357.
(20) Silverman, G. L., Qin, K., Moore, R. C., Yang, Y., Mastrangelo, P., Tremblay, P., Prusiner, S. B., Cohen, F. E., and Westaway, D. (2000) Doppel is an N-glycosylated, glycosylphosphatidylinositol-anchored protein. Expression in testis and ectopic production in the brains of Prnp(0/0) mice predisposed to Purkinje cell loss. *J. Biol. Chem. 275*, 26834−26841.
(21) Luhrs, T., Riek, R., Guntert, P., and Wuthrich, K. (2003) NMR structure of the human doppel protein. *J. Biol. Chem. 326*, 1549−1557.
(22) Baskakov, I. V., Legname, G., Baldwin, M. A., Prusiner, S. B., and Cohen, F. E. (2002) Pathway complexity of prion protein assembly into amyloid. *J. Biol. Chem. 277*, 21140−21148.
(23) Baskakov, I. V., Legname, G., Gryczynski, Z., and Prusiner, S. B. (2004) The peculiar nature of unfolding of the human prion protein. *Protein Sci. 13*, 586−595.
(24) Bocharova, O. V., Breydo, L., Parfenov, A. S., Salnikov, V. V., and Baskakov, I. V. (2005) In vitro conversion of full-length mammalian prion protein produces amyloid form with physical properties of PrP^{Sc}. *J. Mol. Biol. 346*, 645−659.
(25) Tahiri-Alaoui, A., and James, W. (2005) Rapid formation of amyloid from α-monomeric recombinant human PrP in vitro. *Protein Sci. 14*, 942−947.
(26) Post, K., Pitschke, M., Schäfer, O., Wille, H., Appel, T. R., Kirsch, D., Mehlhorn, I., Serban, H., Prusiner, S. B., and Riesner, D. (1998) Rapid acquisition of β-sheet structure in the prion protein prior to multimer formation. *Biol. Chem. 379*, 1307−1317.
(27) Jansen, K., Schäfer, O., Birkmann, E., Post, K., Serban, H., Prusiner, S. B., and Riesner, D. (2001) Structural intermediates in the putative pathway from the cellular prion protein to the pathogenic form. *Biol. Chem. 382*, 683−691.
(28) Leffers, K.-W., Wille, H., Stöhr, J., Junger, E., Prusiner, S. B., and Riesner, D. (2005) Assembly of natural and recombinant prion protein into fibrils. *Biol. Chem. 386*, 569−580.
(29) Eghiaian, F., Daubenfeld, T., Quenet, Y., van Audenhaege, M., Bouin, A.-P., van der Rest, G., Grosclaude, J., and Rezaei, H. (2007) Diversity in prion protein oligomerization pathways results from domain expansion as revealed by hydrogen/deuterium exchange and disulfide linkage. *Proc. Natl. Acad. Sci. U.S.A. 104*, 7414−7419.
(30) Kuwata, K., Li, H., Yamada, H., Legname, G., Prusiner, S. B., Akasaka, K., and James, T. L. (2002) Locally disordered conformer of the hamster prion protein: A crucial intermediate to PrPSc? *Biochemistry 41*, 12277−12283.
(31) Hosszu, L. L. P., Tattum, M. H., Jones, S., Trevitt, C. R., Wells, M. A., Waltho, J. P., Collinge, J., Jackson, G. S., and Clarke, A. R. (2010) The H187R mutation of the human prion protein induces conversion of recombinant prion protein to the PrP^{Sc}-like form. *Biochemistry 49*, 8729−8738.
(32) Yu, H., Liu, X., Neupane, K., Gupta, A. N., Brigley, A. M., Solanki, A., Sosova, I., and Woodside, M. T. (2012) Direct observation of multiple misfolding pathways in a single prion protein molecule. *Proc. Natl. Acad. Sci. U.S.A. 109*, 5283−5288.
(33) Becktel, W. J., and Schellman, J. A. (1987) Protein stability curves. *Biopolymers 26*, 1859−1877.
(34) Swietnicki, W., Petersen, R. B., Gambetti, P., and Surewicz, W. K. (1998) Familial mutations and the thermodynamic stability of the recombinant human prion protein. *J. Biol. Chem. 273*, 31048−31052.
(35) Rezaei, H., Choiset, Y., Eghiaian, F., Treguer, E., Mentre, P., Debey, P., Grosclaude, J., and Haertle, T. (2002) Amyloidogenic unfolding intermediates differentiate sheep prion protein variants. *J. Mol. Biol. 322*, 799−814.
(36) Whyte, S. M., Sylvester, I. D., Martin, S. R., Gill, A. C., Wopfner, F., Schätzl, H. M., Dodson, G. G., and Bayley, P. M. (2003) Stability and conformational properties of doppel, a prion-like protein, and its single-disulphide mutant. *Biochem. J. 373*, 485−494.
(37) Lu, K., Wang, W., Xie, Z., Wong, B. S., Li, R., Petersen, R. B., Sy, M. S., and Chen, S. G. (2000) Expression and structural characterization of the recombinant human doppel protein. *Biochemistry 39*, 13575−13583.
(38) Nicholson, E. M., Mo, H., Prusiner, S. B., Cohen, F. E., and Marqusee, S. (2002) Differences between the prion protein and its homolog Doppel: A partially structured state with implications for scrapie formation. *J. Mol. Biol. 316*, 807−815.
(39) Baillod, P., Garrec, J., Colombo, M.-C., Tavernelli, I., and Rothlisberger, U. (2012) Enhanced sampling molecular dynamics identifies PrP^{Sc} structures harboring a C-terminal β-core. *Biochemistry 51*, 9891−9899.
(40) Colacino, S., Tiana, G., and Colombo, G. (2006) Similar folds with different stabilization mechanisms: The cases of Prion and Doppel proteins. *BMC Struct. Biol. 6*, 17.
(41) Settanni, G., Hoang, T. X., Micheletti, C., and Maritan, A. (2002) Folding pathways of prion and doppel. *Biophys. J. 83*, 3533−3541.
(42) Swietnicki, W., Petersen, R., Gambetti, P., and Surewicz, W. K. (1997) pH-dependent stability and conformation of the recombinant human prion protein PrP(90−231). *J. Biol. Chem. 272*, 27517−27520.
(43) Hornemann, S., and Glockshuber, R. (1998) A scrapie-like unfolding intermediate of the prion protein domain PrP(121−231) induced by acidic pH. *Proc. Natl. Acad. Sci. U.S.A. 95*, 6010−6014.
(44) Gerber, R., Tahiri-Alaoui, A., Hore, P. J., and James, W. (2008) Conformational pH dependence of intermediate states during oligomerization of the human prion protein. *Protein Sci. 17*, 537−544.
(45) Adrover, M., Pauwels, K., Prigent, S., de Chiara, C., Xu, Z., Chapuis, C., Pastore, A., and Rezaei, H. (2010) Prion fibrillization is mediated by a native structural element that comprises helices H2 and H3. *J. Biol. Chem. 285*, 21004−21012.
(46) Alonso, D., DeArmond, S., Cohen, F., and Daggett, V. (2001) Mapping the early steps in the pH-induced conformational conversion of the prion protein. *Proc. Natl. Acad. Sci. U.S.A. 98*, 2985−2989.
(47) DeMarco, M., and Daggett, V. (2004) From conversion to aggregation: Protofibril formation of the prion protein. *Proc. Natl. Acad. Sci. U.S.A. 101*, 2293−2298.
(48) Langella, E., Improta, R., Crescenzi, O., and Barone, V. (2006) Assessing the acid-base and conformational properties of histidine residues in human prion protein (125−228) by means of pK_a calculations and molecular dynamics simulations. *Protein 64*, 167−177.

(49) Campos, S. R. R., Machuqueiro, M., and Baptista, A. M. (2010) Constant-pH Molecular Dynamics Simulations Reveal a β-Rich Form of the Human Prion Protein. *J. Phys. Chem. B 114*, 12692−12700.
(50) van der Kamp, M. W., and Daggett, V. (2010) Influence of pH on the Human Prion Protein: Insights into the Early Steps of Misfolding. *Biophys. J. 99*, 2289−2298.
(51) Garrec, J., Tavernelli, I., and Rothlisberger, U. (2013) Two Misfolding Routes for the Prion Protein around pH 4.5. *PLoS Comput. Biol. 9*, e1003057.
(52) Antosiewicz, J., McCammon, J. A., and Gilson, M. K. (1994) Prediction of pH-dependent properties of proteins. *J. Mol. Biol. 238*, 415−436.
(53) Davis, M., and McCammon, J. (1990) Electrostatics in biomolecular structure and dynamics. *Chem. Rev. 90*, 509−521.
(54) Yang, A., Gunner, M., Sampogna, R., Sharp, R., and Honig, B. (1993) On the calculation of pKa in proteins. *Proteins 15*, 252−256.
(55) Vriend, G. (1990) WHAT IF: A molecular modeling and drug design program. *J. Mol. Graphics 8*, 29 , 52−56.
(56) Spoel, D. V. D., Lindahl, E., Hess, B., Groenhof, G., Mark, A. E., and Berendsen, H. J. C. (2005) GROMACS: Fast, flexible, and free. *J. Comput. Chem. 26*, 1701−1718.
(57) van Gunstern, W., Billeter, S., Eising, A., Huenenberger, P., Krueger, P., Mark, A., Scott, W., and Tironi, I. (1996) *Biomolecular Simulation: The GROMOS96 Manual and User Guide*, Hochschulverlag AG, Zurich.
(58) Berendsen, H., Postma, J., van Gunsteren, W., and Hermans, J. (1981) in *Intermolecular Forces* (Pullman, B. E., Ed.) Reidel, Dordrecht, The Netherlands.
(59) Okur, A., Wickstrom, L., Layten, M., Geney, R., Song, K., Hornak, V., and Simmerling, C. (2006) Improved Efficiency of Replica Exchange Simulations through Use of a Hybrid Explicit/Implicit Solvation Model. *J. Chem. Theory Comput. 2*, 420−433.
(60) Yuguang, M., and Ye, Y. (2005) *NIC Series*, John von Neumann Institute for Computing: Juelich, Germany; Vol. *34*, pp 119−124.
(61) Cheng, X., Cui, G., Hornak, V., and Simmerling, C. (2005) Modified replica exchange simulation methods for local structure refinement. *J. Phys. Chem. B 109*, 8220−8230.
(62) Wang, J., Zhu, W., Li, G., and Hansmann, U. H. E. (2011) Velocity-scaling optimized replica exchange molecular dynamics of proteins in a hybrid explicit/implicit solvent. *J. Chem. Phys. 135*, 084115.
(63) Shell, M. S., Panagiotopoulos, A., and Pohorille, A. (2007) in *Free energy calculations* (Chipot, C., and Pohorille, A., Eds.) Chapter 3, p 85, Springer, Berlin.
(64) Kabsch, W., and Sander, C. (1983) Dictionary of protein secondary structure: Pattern recognition of hydrogen-bonded and geometrical features. *Biopolymers 22*, 2577−2637.
(65) Nguyen, P. H., Li, M. S., and Derreumaux, P. (2011) Effects of all-atom force fields on amyloid oligomerization: Replica exchange molecular dynamics simulations of the Aβ(16−22) dimer and trimer. *Phys. Chem. Chem. Phys. 13*, 9778−88.
(66) Guijarro, J. I., Sunde, M., Jones, J. A., Campbell, I. D., and Dobson, C. M. (1998) Amyloid fibril formation by an SH3 domain. *Proc. Natl. Acad. Sci. U.S.A. 95*, 4224−4228.
(67) Chiti, F., Webster, P., Taddei, N., Clark, A., Stefani, M., Ramponi, G., and Dobson, C. M. (1999) Designing conditions for in vitro formation of amyloid protofilaments and fibrils. *Proc. Natl. Acad. Sci. U.S.A. 96*, 3590−3594.
(68) Chiti, F., Taddei, N., Bucciantini, M., White, P., Ramponi, G., and Dobson, C. M. (2000) Mutational analysis of the propensity for amyloid formation by a globular protein. *EMBO J. 19*, 1441−1449.
(69) Ramirez-Alvarado, M., Merkel, J. S., and Regan, L. (2000) A systematic exploration of the influence of the protein stability on amyloid fibril formation in vitro. *Proc. Natl. Acad. Sci. U.S.A. 97*, 8979−8984.
(70) Yutani, K., Takayama, G., Goda, S., Yamagata, Y., Maki, S., Namba, K., Tsunasawa, S., and Ogasahara, K. (2000) The process of amyloid-like fibril formation by methionine aminopeptidase from a hyperthermophile, *Pyrococcus furiosus*. *Biochemistry 39*, 2769−2777.
(71) Kuwata, K., Kamatari, Y. O., Akasaka, K., and James, T. L. (2004) Slow conformational dynamics in the hamster prion protein. *Biochemistry 43*, 4439−4446.
(72) Lu, X., Wintrode, P. L., and Surewicz, W. K. (2007) β-Sheet core of human prion protein amyloid fibrils as determined by hydrogen/deuterium exchange. *Proc. Natl. Acad. Sci. U.S.A. 104*, 1510−1515.
(73) Fitzmaurice, T. J., Burke, D. F., Hopkins, L., Yang, S., Yu, S., Sy, M.-S., Thackray, A. M., and Bujdoso, R. (2008) The stability and aggregation of ovine prion protein associated with classical and atypical scrapie correlates with the ease of unwinding of helix-2. *Biochem. J. 409*, 367−375.
(74) Xu, Z., Prigent, S., Deslys, J.-P., and Rezaei, H. (2011) Dual conformation of H2H3 domain of prion protein in mammalian cells. *J. Biol. Chem. 286*, 40060−40068.
(75) Dima, R. I., and Thirumalai, D. (2004) Probing the instabilities in the dynamics of helical fragments from mouse PrPC. *Proc. Natl. Acad. Sci. U.S.A. 101*, 15335−15340.
(76) Simone, A. D., Zagari, A., and Derreumaux, P. (2007) Structural and hydration properties of the partially unfolded states of the prion protein. *Biophys. J. 93*, 1284−1292.
(77) Santini, S., and Derreumaux, P. (2004) Helix H1 of the prion protein is rather stable against environmental perturbations: Molecular dynamics of mutation and deletion variants of PrP(90−231). *Cell. Mol. Life Sci. 61*, 951−960.
(78) Chebaro, Y., Pasquali, S., and Derreumaux, P. (2012) The Coarse-Grained OPEP Force Field for Non-Amyloid and Amyloid Proteins. *J. Phys. Chem. B 116*, 8741−8752.
(79) Kuznetsov, I. B., and Rackovsky, S. (2004) Comparative computational analysis of prion proteins reveals two fragments with unusual structural properties and a pattern of increase in hydrophobicity associated with disease-promoting mutations. *Protein Sci. 13*, 3230−3244.
(80) Bocharova, O. V., Breydo, L., Salnikov, V. V., Gill, A. C., and Baskakov, I. V. (2005) Synthetic prions generated in vitro are similar to a newly identified subpopulation of PrPSc from sporadic Creutzfeldt-Jakob disease. *Protein Sci. 14*, 1222−1232.
(81) Cobb, N. J., Sönnichsen, F. D., McHaourab, H., and Surewicz, W. K. (2007) Molecular architecture of human prion protein amyloid: A parallel, in-register β-structure. *Proc. Natl. Acad. Sci. U.S.A. 104*, 18946−18951.
(82) Baskakov, I. V., Legname, G., Prusiner, S. B., and Cohen, F. E. (2001) Folding of prion protein to its native α-helical conformation is under kinetic control. *J. Biol. Chem. 276*, 19687−19690.